HiSST: 3rd International Conference on
High-Speed Vehicle Science Technology
14 -19 April 2024, Busan, Korea

Three-dimensional curved conical shock wave/plate boundary layer interactions

Jianrui Cheng[1], Chongguang Shi[1], Xiaogang Zheng[1], Chengxiang Zhu[1], Yancheng You[1]

Abstract

In practical aerodynamic scenarios, interactions between curved shock waves and boundary layers exhibiting composite shock curvatures in both streamwise and spanwise directions occur more frequently than those induced by planar oblique shocks. To gain a more systematic understanding of this phenomenon, the three-dimensional curved shock wave/boundary layer interactions (CSBLI) with a curved cone above plate are studied using CFD method with RANS equations. The effects of straight, convex, and concave conical shock waves inducing separation are compared in sections of different directions, reflecting the influence of shock wave on the streamwise and spanwise scales of three-dimensional separation synchronously. Finally, the Mach reflection on both sides of the curved conical shock wave is analyzed by comparing with the inviscid conditions, indicating that the viscous separation bubble can delay the occurrence of Mach reflection.

Keyword: *Curved shock wave, Shock wave/boundary layer interaction, Flow structure, Flow separation, Reynolds-averaged*

Nomenclature

Re – Reynolds number
Ma – Mach number
δ_0 – Boundary layer thickness
L – Length
x_c – Distance of the apex
h – Height of the apex
θ – Half-cone angle
c_f – Wall friction coefficient
p – Pressure
τ_w – Wall shear stress
Subscripts
x/y/z – x-/y-/x-direction
∞ – Incoming flow
w – Wall
0 – Initial
1 – Terminal

1. Introduction

Shock wave/boundary layer interactions (SBLI) are common in both internal and external supersonic aerodynamic configurations. Due to the thickening and potential separation of the boundary layer resulting from adverse pressure gradients, SBLI often has a detrimental effect on flow performance, causing a range of issues such as flow distortion, localized hyperthermia, and structural oscillations [1]. As a result, over the past few decades, research into SBLI has explored various aspects, including separation scales [2], flow field structures [3], unsteady characteristics [4] and flow control [5].

As a model abstracted from engineering, one of the canonical SBLI configurations with a cone above plate is frequently encountered in the inward-turning inlets or the conical cowlings of high-speed vehicles. The resultant conical shock wave/boundary layer interactions (CSBLI) exhibit typical flow characteristics, with axisymmetric flow occurring after conical shock wave and three-dimensional separation near plate. This flow topological structure was studied firstly by Panov experimentally with a freestream Mach number of 2.87 [6], wherein the separation line and reattachment line were observed, along with a convex separation region. Gai and Teh conducted an experimental study of CSBLI at a freestream Mach number of 2.0 [7]. By varying the half-angle of the cone, a corresponding

[1] *Xiamen University, Xiamen, Fujian, China, chengjr@stu.xmu.edu.cn*

variation of three-dimensional separation was achieved, which reduced in size away from symmetry plane. Hale synthetically utilized surface oil flow, pressure-sensitive paint (PSP) and particle image velocimetry (PIV) to conduct an experiment on CSBLI with an incoming Mach number of 2.05, studying the interactions from multiple aspects [8]. In the symmetry plane, a quasi-two-dimensional flow was observed, while three-dimensional separation extended to both sides from this region. These experimental conditions and results provided abundant data for the following studies. Zuo et al. adopted direct numerical simulations (DNS) on CSBLI at a lower Reynolds number [9-10]. The development of fine vortex structures within boundary layer was observed, and statistical analysis revealed the mean and instantaneous characteristics of separation. Additionally, Zuo et al. also conducted the Reynolds-averaged numerical simulations (RANS) for the calculation of CSBLI flow [11-12]. The RANS method proved effective in capturing separation flow and wall parameter distribution, as demonstrated by comparison with experimental data in higher Reynolds number ($Re_{\delta 0} \approx 55500$, based on the boundary layer thickness) and DNS data in lower Reynolds number ($Re_{\delta 0} \approx 7000$), utilizing appropriate turbulence models. In addition to these aforementioned work, the pressure fluctuations of different separation regions have been studied based on the DNS database by Zuo et al. [13-14], elucidating the unsteady features of CSBLI flow structures in frequency domain.

Although the CSBLI flow has been extensively studied in terms of separation scales, parameter distributions, shock wave structures and unsteady oscillations, this abstracted model of a straight cone cannot fully describe the common phenomenon of SBLI induced by curved conical forebodies in engineering applications, such as the design of supersonic aircraft with conical cowling. Therefore, it remains a problem that the three-dimensional non-uniform flow after curved conical shock waves has a different influence on separation in practical aerodynamic scenarios. Thus, a more complicated flow model that considers the interaction between curved conical shock wave and plate boundary layers is proposed. The streamwise and spanwise curvatures of shock waves have been demonstrated analytically to have an influence on separation scales in two-dimensional plane SBLI and axisymmetric SBLI [15,16]. It is necessary to investigate the three-dimensional effects caused by composite shock wave curvatures.

In the present study, the CSBLI is analyzed using CFD method with RANS equations under different configurations, with cones having convex, concave, and straight generatrixes, located above a flat plate respectively. The numerical simulation method is introduced in Section 2 with multifaceted verifications. The results and discussions are described in Section 3, including the discussion of Mach reflection in CSBLI. Conclusions are provided in Section 4.

2. Description of numerical simulation method

In the range of studied flow properties ($Re_{\delta 0} \approx 45000$), there is currently a relative lack of DNS data available for SBLI. High-precision numerical simulations such as DNS and LES are typically applied to flows with lower Reynolds numbers, as turbulent flow fields can be better resolved in such cases. However, flows with higher Reynolds numbers often feature microscale structures that are beyond the computational power [17-19]. Therefore, considering the comprehensive understanding of the flow field characteristics and summary of regularities, the RANS equations are applied in the present study. Firstly, the numerical methods are verified based on the experimental model of Gai and Teh [7], which featured an incoming Mach number of 2.0 and a Reynolds number of 55500 based on boundary layer thickness. This model was also studied numerically by Zuo et al. [11]. The computational domain is identical in scale to Ref.[11] in order to facilitate comparison, with L_x = 300 mm, L_y = 120 mm and L_z = 60 mm. A straight cone is located above a plate with the apex and leading edge positioned at a distance of x_c = 80mm, and a height of h = 30 mm, as shown in Fig.1(a). To simplify the calculations, the domain is taken as a half module where the corresponding boundary condition is set as a symmetry plane.

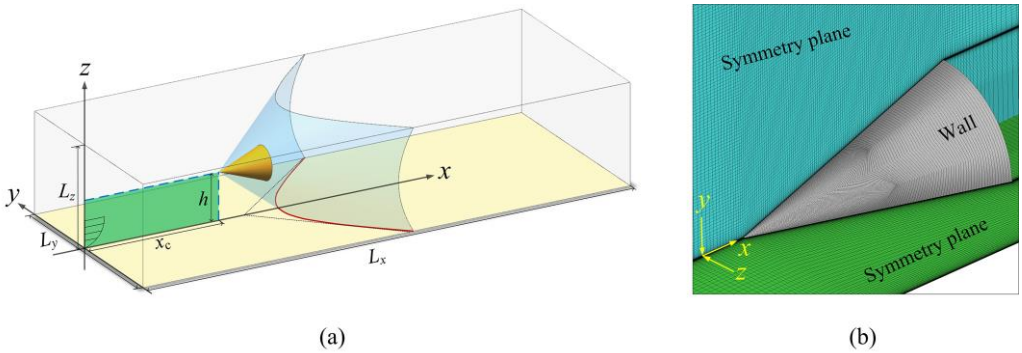

Fig 1. Computational domain and block-structured grid

The computational domain is discretized using a block-structured grid, which is refined in the wall-normal direction to ensure $y^+ < 1$ near the wall. Different turbulence models are selected for the calculations to test their ability to capture boundary layer separation. Fig.2 compares the pressure and friction coefficient distributions along wall in the symmetry plane with the experimental results from Ref.[7] and the numerical results from Ref.[11], where the half-cone angles are θ = 14°, 20° and 30° respectively, showing that the RANS equations can effectively capture the pressure rising and separation scales.

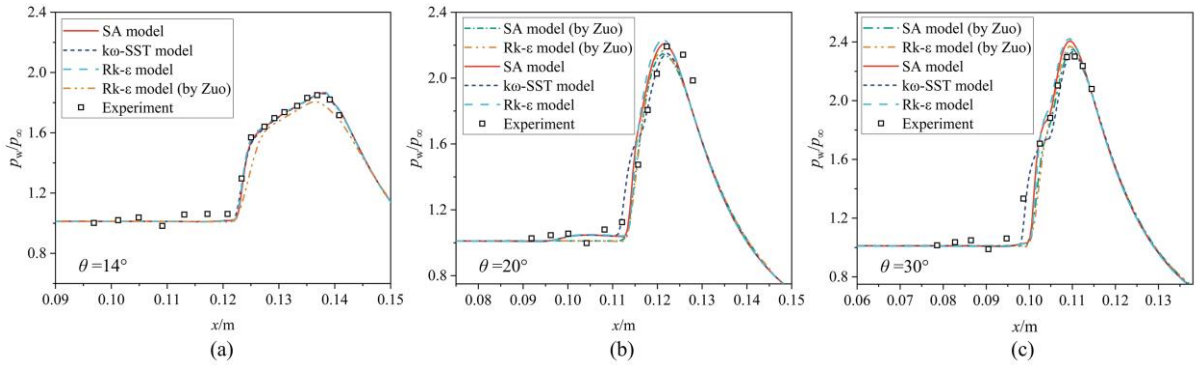

Fig 2. Verification of turbulence models with straight cone above plate

For the model of θ = 20°, verification of grid independence is also carried out by comparing the friction coefficient and pressure distributions along wall in the symmetry plane, as shown in Fig.3. The light-blue solid lines represent the results calculated by the coarse grid, which has approximated 10 million cells. The results of fine grid with about 16 million cells are illustrated as red dash-dotted lines, and those of dense grid with about 20 million cells are shown in dark-blue dash lines. Convergence is achieved using fine grid, which will be subsequently used in the following cases.

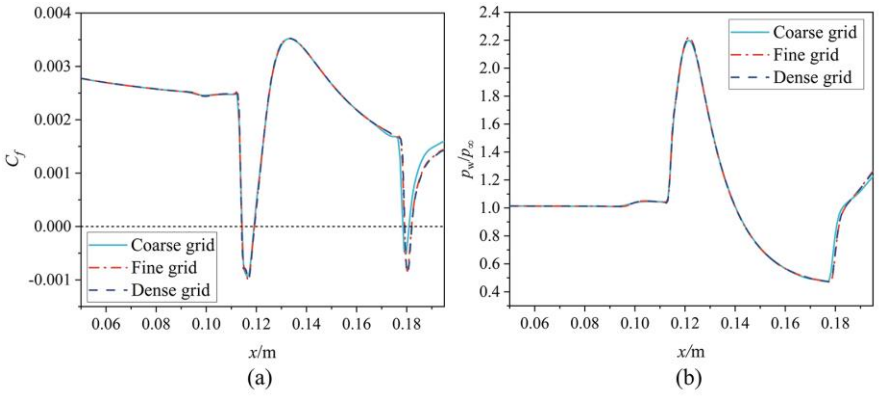

Fig 3. Verification of grid independence

3. Results and discussion

Several cases are examined to explore the influence of three-dimensional curved shock waves on separation, using curved cones with different concave and convex generatrixes as shock generators. These generatrixes are described with initial half-cone angles (θ_0) and terminal deflection angles (θ_1), and spline curves are used to connect both endpoints. The geometry parameters of these generatrixes are listed in Tab.1, and illustrated in Fig.4. The distance between the apex and leading edge of the plate remains at x_c = 80mm, but the height of symmetry axis reduces to h = 20mm to ensure that the separation region is upstream of the expansion waves. Unlike the cases presented in Section 2, the incoming Mach number and Reynolds number are set as Ma_∞ = 3 and $Re_{\delta_0} \approx$ 60000 respectively, in order to induce separation with sufficient scales.

Table 1. Geometrical parameters of curved cones

Case	Initial half-cone angle (degree)	Terminal deflection angle (degree)
1	20	20
2	10	30
3	5	30
4	10	40
5	30	10
6	30	5
7	40	10

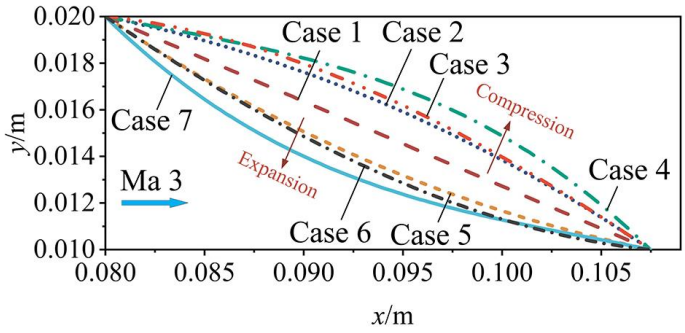

Fig 4. Generatrixes of curved cones

In Case 1, a straight cone with a half-cone angle of 20° is used as a comparison. In Cases 2 to 4, concave cones are considered, while convex cones are examined in Cases 5 to 7. According to the curved shock theories (CST) [20], an isentropic compression is induced from Cases 2 to 4, generating a concave conical shock wave, while an isentropic expansion is created from Cases 5 to 7, leading to a convex conical shock wave. Interacting with the incoming boundary layer on the plate, three-dimensional CSBLI is generated. Fig.5 displays the contours of Mach number on symmetry plane for these cases, reflecting the main structures of CSBLI.

In Case 1, a canonical CSBLI is induced by the straight cone, exhibiting a flow structure similar to that calculated in previous study by Zuo et al.[11]. The flow can be treated as a semi-two-dimensional SBLI on the symmetry plane, with a streamwise separation length of 5.27mm measured as the distance between the separation and reattachment points on the symmetry plane [11]. In Cases 2 and 3, curved shock waves with concave shapes facing upstream are induced, resulting in a semi-two-dimensional CSBLI that is similar to the flow studied in Ref.[15]. The separation lengths in both cases are 7.48mm and 7.76mm respectively. However, a unique phenomenon is observed in Case 4. The excessively large value of the half-cone angle at the end of the cone causes a substantial expansion downstream, resulting in a higher pressure ratio. This, in turn, causes a larger shock angle for the lower section and exacerbated the separation of the boundary layer up to 9.84mm due to this higher adverse pressure gradient. Moreover, in Cases 5 to 7, convex conical shock waves are generated, and the streamwise

separation lengths are measured as 3.28mm, 3.81mm, and 3.31mm, respectively. From Case 1 to Case 4, the reflected shock waves can be clearly observed due to the relatively stronger shock impingement. Compared to the inviscid conical shock reflection, the reflected shock waves can appear in two forms: transmitted waves that interact with separation shocks upstream and reattachment shocks downstream. However, in Cases 5 to 7, both reflected shocks are weaker and coupled, due to the small separation scales.

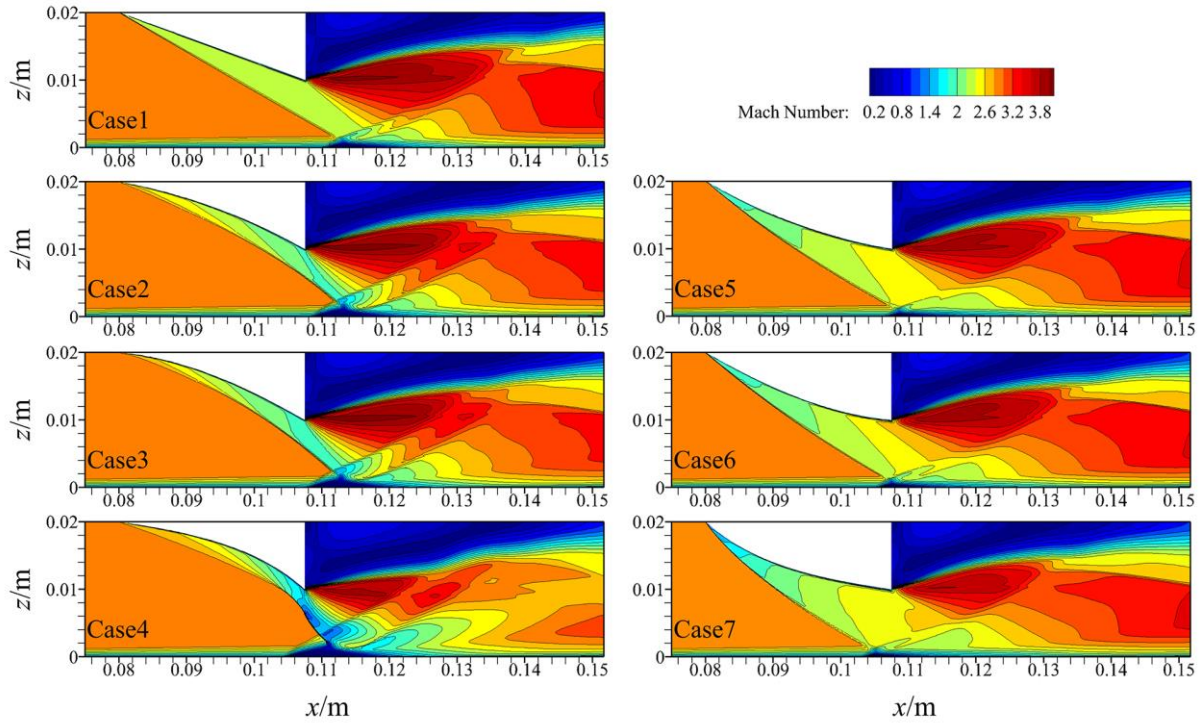

Fig 5. Contours of Mach number in x-z plane of each case

The pressure and friction coefficient distributions along wall on symmetry planes in these cases are quantitatively compared and illustrated in Fig.6(a) and (b) respectively. Notable differences exist in the impingement of concave and convex shock waves. In Cases 2 to 4, higher normalized pressure peaks are calculated, with values of 4.90, 5.04 and 5.42, with an almost isobaric pressure platform upstream in each case. After the peaks, the flow undergoes a period of dramatic expansion to reach a state of pressure equilibrium. However, in Cases 5 to 7, with smaller shock foot angles, the normalized pressure peaks are lower with values of 3.46, 3.64 and 3.34 respectively. A gentler expansion acts on the flow in each case after reattachment, eventually achieving the same pressure equilibrium state.

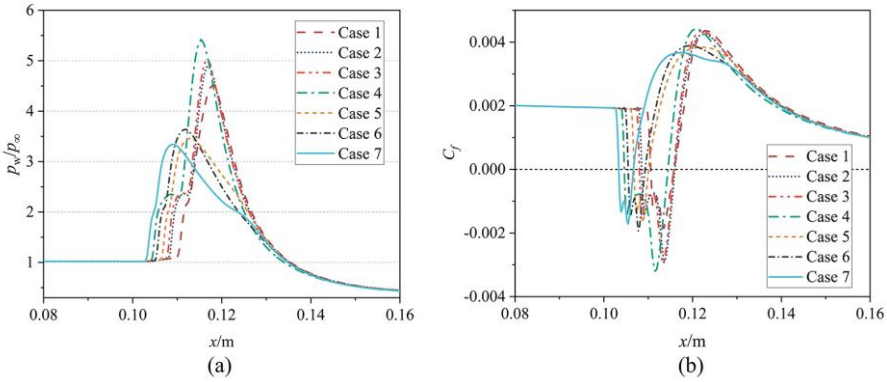

Fig 6. Distributions of pressure and wall friction coefficients along wall in symmetry plane

From another perspective, since the separations induced by CSBLI are three-dimensional in nature, the spanwise scales of separation regions are also influenced by the curved surfaces of shock waves. Fig.7 depicts the limiting streamlines and pressure contours on the wall of x-y plane in each case, reflecting

the entire separations in both streamwise and spanwise directions. The upstream separation line and downstream reattachment line in each case exhibit obvious U-shapes, similar to the inviscid reflection line of the conical shock wave on a plate. Between these lines, the flow reverses towards both opposite and transverse directions. A high-pressure area appears near the reattachment line and extends from the symmetry plane to both sides and gradually diminishes.

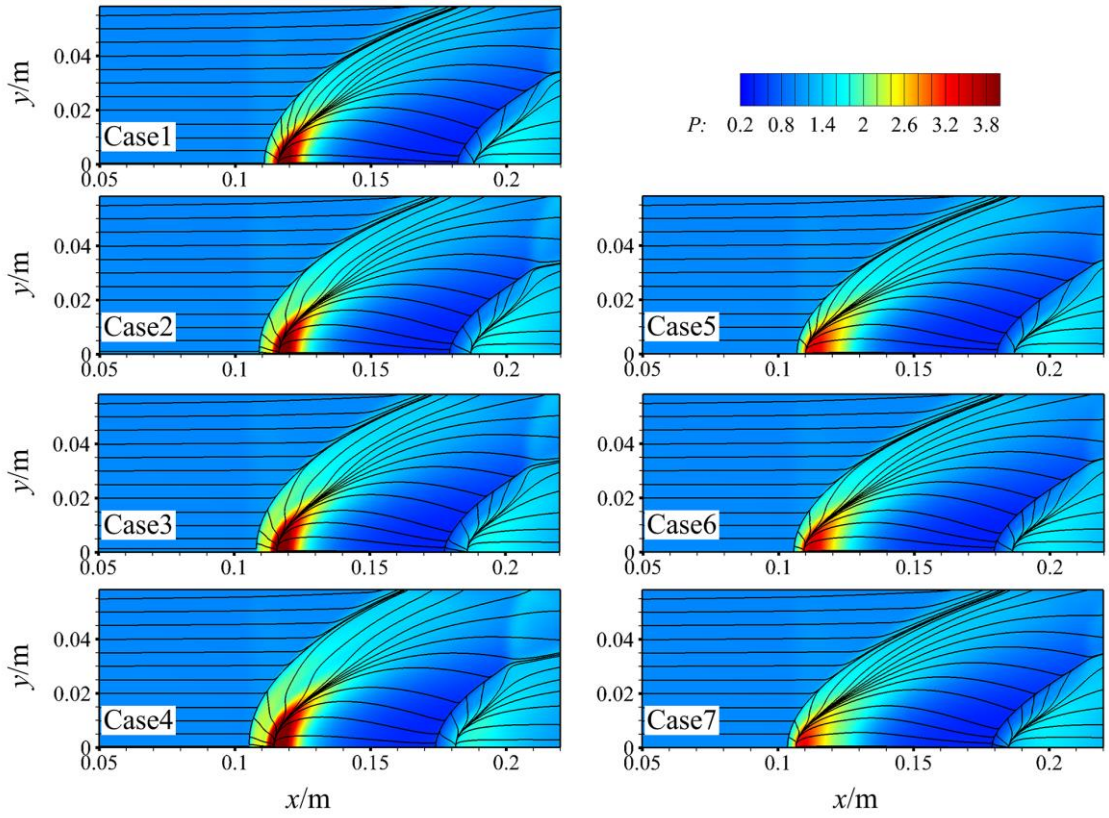

Fig 7. Limiting streamlines and pressure contours in x-y plane of each case

As the swept angle of incident shock wave in the spanwise y direction increases, the pressure-rising effect on the incoming flow gradually diminishes [21]. To define the geometries of separation bubbles, the shapes of separation lines are extracted and analyzed. In Fig.8(a), the limiting streamlines are traced, and the points where sharp deflections occur are depicted in Fig.8(a) as scatter. The deflection points can be fitted accurately to a hyperbolic curve as the form of $y = (a^2(x-c)^2-b^2)^{0.5}$, with $R^2 > 0.99$ for all the cases, where a, b and c are undetermined coefficients. This indicates that the leading-edges of separations induced by curved conical shock waves with different geometries can closely approximate hyperbolic shapes. All the separation lines in Fig.8(a) are displaced onto the same starting point to allow for a direct comparison of the sweepback angles.

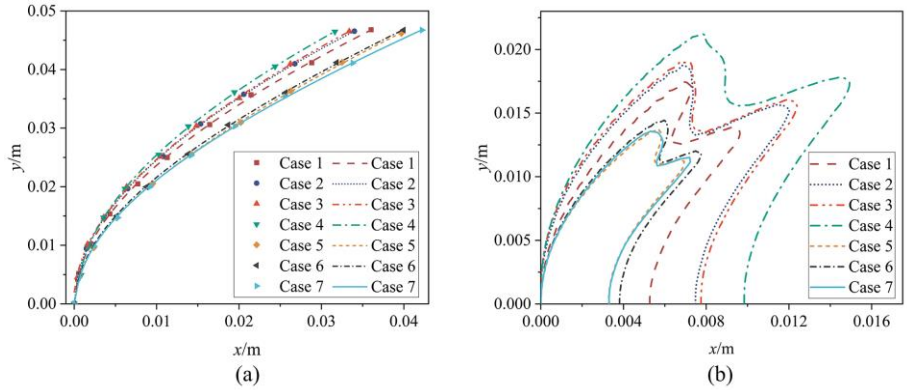

Fig 8. Separation lines and outline of separation bubbles

In Fig.8(a), all the swept leading-edges can be classified into three categories based on their sweepback angles. The curves in Cases 2-4 expand more towards the lateral direction and have smaller sweep angles. In contrast, those in Cases 5-7 have larger sweep angles. In Case 1, the leading-edge induced by conical shock wave falls between these two categories. The distribution of leading-edges shows that the concave incident shock wave induces a relatively wider separation region with a smaller sweepback angle, while the opposite is true for the convex one. In previous studies on two-dimensional SBLI, the separation length scales in the streamwise direction have been thoroughly discussed and are believed to depend on the strength and curvature of shock wave [15, 22-23]. However, Fig.8(a) demonstrates that the separation scales in the spanwise direction are also related to the incident shock waves, as reflected in their sweepback characteristics. The separation scales induced by concave conical shock waves are wider in spanwise direction than those induced by convex ones, and the same pattern applies to the streamwise separation scales.

It appears that both the streamwise and spanwise separation scales are influenced by the composite curved characteristics. Thus, the approximately complete separation zone in each case is illustrated in Fig.8(b), with the boundary defined by $\tau_{wx} = 0$. While zero skin-friction values cannot completely capture three-dimensional separation [1], the region defined by this frame can more comprehensively reflect the relative sizes of the three-dimensional separation scales projected onto the wall [12]. In Fig.8(b), the region bounded by each curve represents the zone of reverse flow. The projection regions of all the cases are geometrically similar, with a trend of both enlargement and shrinkage observed the streamwise and spanwise directions.

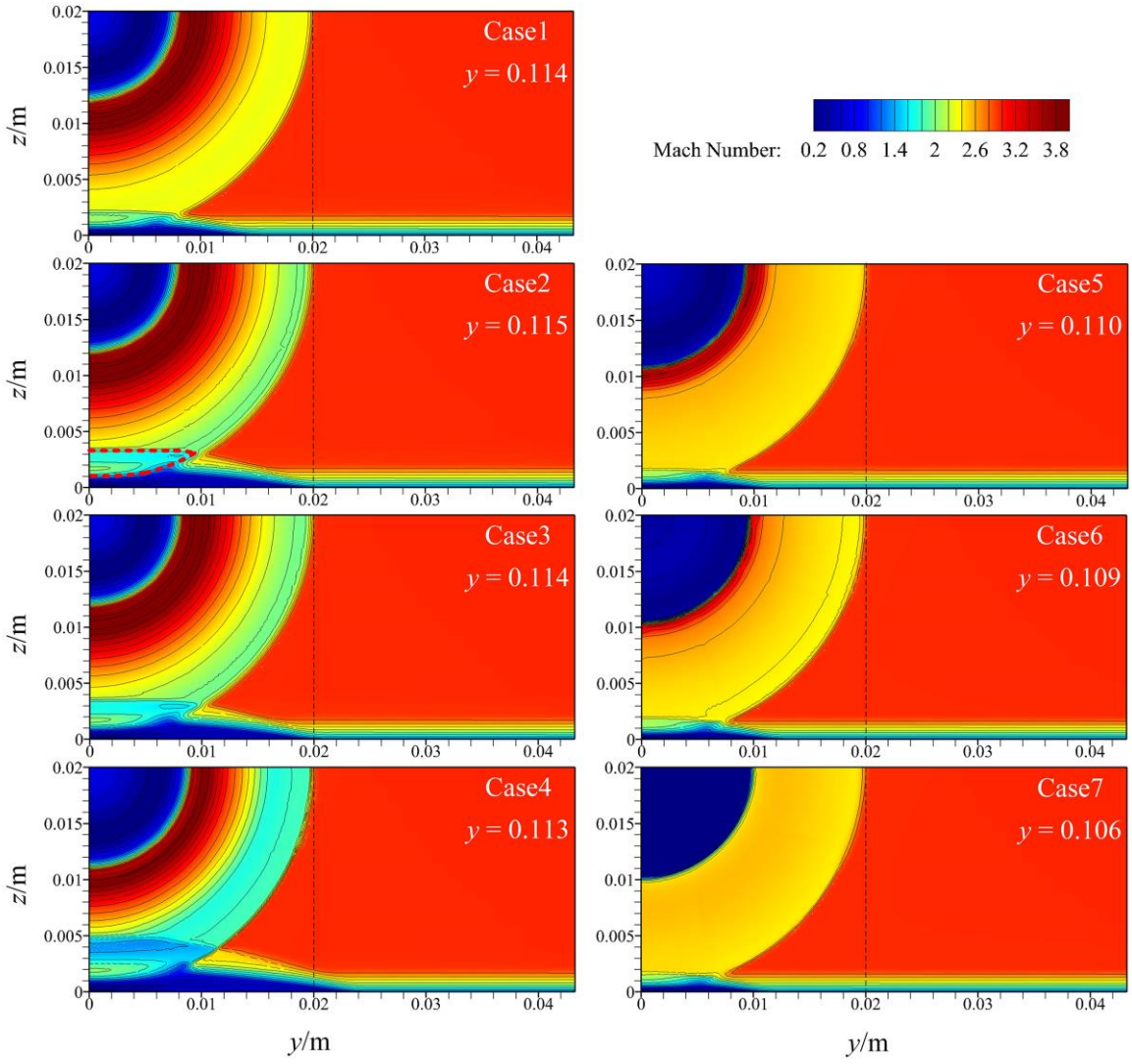

Fig 9. Contours of Mach number in y-z plane of each case

To demonstrate the influence of different curved conical shock waves more clearly on the spanwise characteristics of separations, the x-z plane of each case where the incident shock wave just reaches the wall in the hypothetical case of inviscid flow is extracted and illustrated in Fig.9. Therefore, the incident shock wave appears as a circle with a radius of 0.02m by observing from the plane perpendicular to the incoming flow. Under the impact of the adverse pressure gradient, the boundary layer gradually lifts from both sides toward the center and finally separates near the symmetry plane. In each case, there exist two distinct boundaries above the separation regions, marking with red dash-lines in Case 2 as an example, emitting from the positions close to z = 0.001 and 0.003 respectively and intersecting at the location of x ≈ 0.01. Comparing with Fig.6, the upper boundary is the transmitted shock wave generated by interaction between upstream separated shock wave and incident shock wave, presenting a convex shape. The lower boundary is the starting line of the reattachment shock wave, presenting a concave shape. Thus, combining the two perspectives from Fig.5 and Fig.11 allows for a clearer assessment of the three-dimensional surface shapes of the transmitted and reattachment shock waves. The leeside of the separation bubble is located between these two shock waves, causing expansion of the flow. Generally, for concave incident shock waves, Cases 2-4 have relatively large expansion regions due to the higher height of the separation bubbles and the more intense strength of the reflected shock waves. But for convex incident shock waves, the smaller separations and weaker reflected shock waves result in smaller expansion regions in Cases 5-7.

The pressure and skin-friction coefficient distributions along wall in spanwise direction on each plane are extracted in Fig.10(a) and (b). The spanwise scales of separations are related to the spanwise distributions of pressure applied to boundary layer by shock waves. From the symmetry plane, the pressure decreases gradually from the peak, corresponding to the gradual decrease of the shock wave spanwise intensity [24]. Under this condition, intense separation with negative values of C_f occurs near the symmetrical plane. Subsequently, similar to the streamwise pressure distribution, a relatively stable pressure platform appears following the high-pressure region, where the flow is more uniform and corresponding value of skin-friction coefficient remains almost constant as well. Finally, as passing the region influenced by adverse pressure gradient, the pressure gradually decreases and approaches the freestream value. At this point, C_f passes through zero and the reverse flow gradually disappears, and the boundary layer near the outer side no longer separates under these conditions.

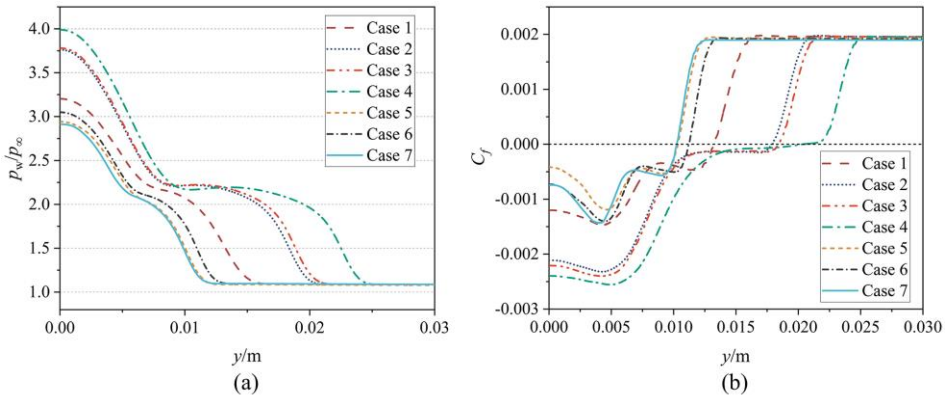

Fig 10. Distributions of pressure and wall friction coefficient along wall in y-z section of each case

Through the above analyses, a more comprehensive understanding of the interaction structures has been gained. However, the shock wave system exhibits a more complex relevance compared to the two-dimensional SBLI, especially with regards to Mach reflections on both sides [24]. When an inviscid assumption is made, the reflection lines of these curved shock waves on a wall actually can be calculated directly using Eq.(1) with the analytical geometry method.

$$(z-h)^2 + y^2 = \left(h - f(x)\right)^2 \tag{1}$$

$$z = 0$$

In Eq.(1), x, y, z are coordinate values, and the shock wave curve in symmetry plane is described by z = f(x). h is the height of the axis of cone. For the straight conical shock wave, f(x) is a linear function, and the shock reflection line is thus a hyperbolic line. By ignoring the possibility of Mach reflection occurring on both sides, the hypothetical inviscid shock reflection lines are illustrated in Fig.11(b).

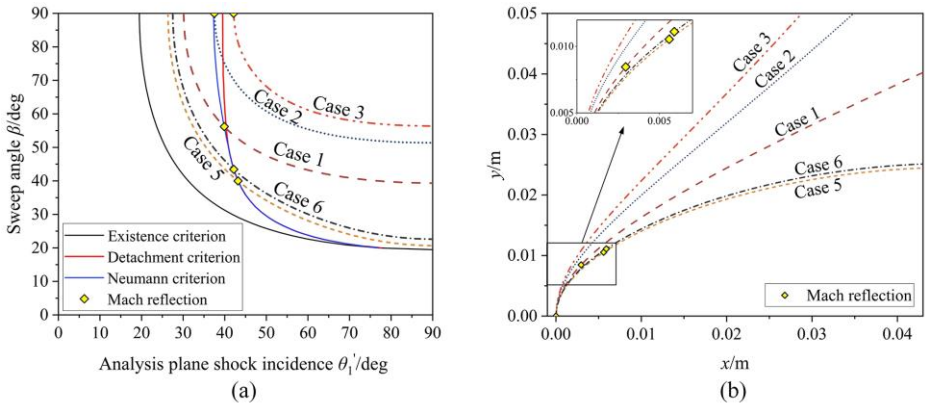

Fig 11. Criteria for existence and transition between Mach and regular reflection in each case

However, under real circumstances, Mach reflection occurs as the sweep angle increases. For an incoming Mach number of 3, the criteria for existence and transition between Mach and regular reflection are shown in Fig.11(a) [24]. The yellow point of each case reflects the location where Mach reflection happens, which has also been marked in Fig.11(b). It shows that the Mach reflection points are all very close to the symmetry plane, especially in Case 2 and Case 3 induced by concave shock waves where no regular reflection exists. But in the viscous CSBLI, there are some points of transition between Mach and regular reflections, which are illustrated in Fig.12 respectively. The presence of separation bubble obviously delays the occurrence of Mach reflection, which means that a larger sweepback and larger shock angle in analysis plane can induce Mach reflection due to the intersection between separation shock wave and incident shock wave.

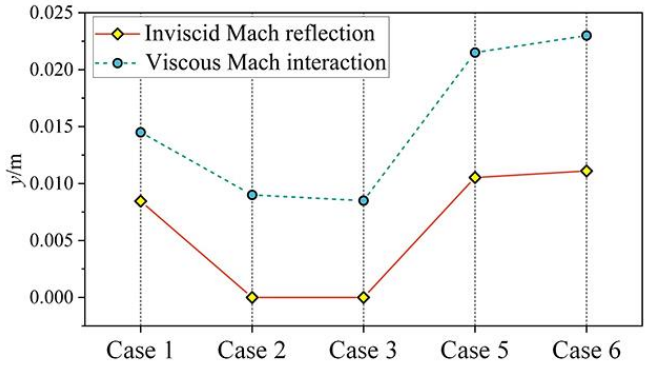

Fig 12. Locations of Mach reflection occurs in inviscid and viscous flow

4. Conclusion

The present study utilizes the CFD method with RANS equations to investigate the flow structures of CSBLI exhibiting composite shock curvatures in both streamwise and spanwise directions. The flow fields resulting from a curved conical shock wave impinging on a plate are analyzed comprehensively from the view of x-z plane, x-y plane and y-z plane respectively.

When compared to straight conical shock waves, concave shock waves cause greater separation due to the isentropic compression that occurs behind incident shock wave, while convex shock waves lead to a decrease in separation due to the expansion behind. These curved characteristics have synchronous effects on both the streamwise and spanwise scales. In addition to affecting separation, from the perspective of y-z section, the intensity and curvature of incident shock wave also act on the reflection shock waves. When a more intense concave shock wave is present, the higher separation bubble leads to the generation of two separated reflection shock waves: the transmitted shock wave and attachment shock wave. However, for a weaker convex shock wave, the two reflection shock waves are closer together and even fuse into a single shock wave.

Despite the multiple impinging lines of the curved conical shock, all the separation lines can be precisely fitted as hyperbolic curves. Mach reflection occurs on both sides as the sweepback angle of shock wave increases, but the presence of a viscous separation bubble delays this trend.

References

1. Datta V. Gaitonde, Michael C. Adler: Dynamics of three-dimensional-shock-wave/boundary-layer interactions. Annu. Rev. Fluid Mech. 55, 291-321 (2023)
2. Huo J, Yi S, Zheng W, et al.: Experimental investigation of expansion effect on shock wave boundary layer interaction near a compression ramp. Chinese J. Aeronaut. 35, 89-101 (2022)
3. Yongyi Zhou, Yilong Zhao, Gang He, et al.: Study on the separation in the shock wave/boundary layer interaction induced by a curved fin. Phys. of Fluids. 35, 076106 (2023)
4. Ceci A, Palumbo A, Larsson J, et al.: On low-frequency unsteadiness in swept shock wave-boundary layer interactions. J. Fluid Mech. 956, R1 (2023)
5. Dake K, Chao Y, Sijia L, et al.: Modelling and shock control for a V-shaped blunt leading edge. J. Fluid Mech. 968, A15 (2023)
6. Panov Y A: Interaction of incident three-dimensional shock with a turbulent boundary layer. Fluid Dyn. 3, 108-110 (1968)
7. S L Gai, S L Teh.: Interaction Between a conical shock wave and a plane turbulent boundary layer. 38, 804-811 (2000)
8. Jason T Hale: Interaction between a conical shock wave and a plane compressible turbulent boundary layer at Mach 2.05. Urbana: University of Illinois at Urbana-Champaign (2015)
9. Zuo F, Memmolo A, Huang G, et al.: Direct numerical simulation of conical shock wave–turbulent boundary layer interaction. J. Fluid Mech. 877, 167-195 (2019)
10. Zuo F: The scaling of separation bubble in the conical shock wave/turbulent boundary layer interaction. Acta Astronaut. 186, 418-425 (2021)
11. Zuo F, Memmolo A, Pirozzoli S: Reynolds-averaged numerical simulations of conical shock-wave/boundary-layer interactions. AIAA J. 59, 1645-1659 (2021)
12. Zuo F: Hypersonic conical shock-wave/turbulent-boundary-layer interaction at higher Reynolds number. AIAA J. 61, 3743-3760 (2023)
13. Zuo F, Yu M, Pirozzoli S: Modal analysis of separation bubble unsteadiness in conical shock wave/turbulent boundary layer interaction. AIAA J. 60 (2022)
14. Zuo F, Memmolo A, Pirozzoli S: On wall pressure fluctuations in conical shock wave/turbulent boundary layer interaction. J. Fluid Mech. 967, A3 (2023)
15. Cheng J, Yang K, Zheng X, et al.: Analytical model for predicting the length scale of shock/boundary layer interaction with curvature. Phys. of Fluids. 34, 111701 (2022)
16. Cheng J, Zhang T, Shi C, et al.: Analytical reconstruction of axisymmetric curved shock wave/boundary layer interactions. Phys. of Fluids. (2024)
17. Zuo F, Wei J, Hu S, et al.: Effects of wall temperature on hypersonic impinging shock-wave/turbulent-boundary-layer interactions. AIAA J. 60 (2022)
18. Bernardini M, Della Posta G, Salvadore F, et al.: Unsteadiness characterisation of shock wave/turbulent boundary-layer interaction at moderate Reynolds number. J. Fluid Mech. 954, A43 (2023)
19. Hu W, Hickel S, Van Oudheusden B: Low-frequency unsteadiness mechanisms in shock wave/turbulent boundary layer interactions over a backward-facing step. J. Fluid Mech. 915, A107 (2021)
20. Sannu Mölder: Curved shock theory. Shock waves. 26, 337-353 (2016)

21. James A S Threadgill, Jesse C Little: An inviscid analysis of swept oblique shock reflections. J. Fluid Mech. 890, A22 (2020)
22. L J Souverein, P G Bakker, P Dupont: A scaling analysis for turbulent shock-wave/ boundary-layer interactions. J. Fluid Mech. 714, 505-535 (2013)
23. Yuting Hong, Zhufei Li, Jiming Yang: Scaling of interaction lengths for hypersonic shock wave/turbulent boundary layer interactions. Chinese J. Aeronaut. 34, 504-509 (2021)
24. Divek Surujhlal, Beric W. Skews: Three-dimensional shock wave reflection transition in steady flow. J. Fluid Mech. 858, 565-587 (2019)
25. H Babinsky, J K Harvey: Shock wave boundary layer interactions. Cambridge University Press (2011)